Nonstabilizerness of neural quantum states

Alessandro Sinibaldi [1,2,*] Antonio Francesco Mello [3,4,†] Mario Collura [3,5] and Giuseppe Carleo [1,2]
[1]Institute of Physics, École Polytechnique Fédérale de Lausanne (EPFL), CH-1015 Lausanne, Switzerland
[2]Center for Quantum Science and Engineering, EPFL, Lausanne, Switzerland
[3]International School for Advanced Studies (SISSA), Via Bonomea 265, I-34136 Trieste, Italy
[4]Center for Computational Quantum Physics, Flatiron Institute, 162 5th Avenue, New York, New York 10010, USA
[5]INFN, Sezione di Trieste, Via Valerio 2, 34127 Trieste, Italy

(Received 26 February 2025; revised 27 May 2025; accepted 12 November 2025; published 12 December 2025)

We introduce a methodology to estimate nonstabilizerness or "magic," a key resource for quantum complexity, with neural quantum states (NQS). Our framework relies on two schemes based on Monte Carlo sampling to quantify nonstabilizerness via stabilizer Rényi entropy (SRE) in arbitrary variational wave functions. When combined with NQS, this approach is effective for systems with strong correlations and in dimensions larger than one, unlike tensor network methods. First, we study the magic content in an ensemble of random NQS, demonstrating that neural network parametrizations of the wave function capture finite nonstabilizerness besides large entanglement. Second, we investigate the nonstabilizerness in the ground state of the J_1-J_2 Heisenberg model. In one dimension, we find that the SRE vanishes at the Majumdar-Ghosh point $J_2 = J_1/2$, consistent with a stabilizer ground state. In two dimensions, a dip in the SRE is observed near maximum frustration around $J_2/J_1 \approx 0.6$, suggesting a valence bond solid between the two antiferromagnetic phases.

DOI: 10.1103/v5tw-yn1f

I. INTRODUCTION

Harnessing the exponential complexity of quantum systems to overcome the limitations of classical computing lies at the heart of quantum advantage. Entanglement has been identified as a fundamental feature that accounts for this complexity and has thus been thoroughly studied as a crucial resource [1–3]. However, it is also well known that entanglement is not the sole resource required to quantify quantum complexity. In particular, an equally essential resource is nonstabilizerness—also known as "magic" [4–6]. The latter describes the degree to which a given quantum protocol diverges from polynomial simulability within the framework of the Gottesman-Knill theorem.

Although several measures of nonstabilizerness have been proposed [7–9], evaluating most of these nonstabilizerness monotones remains computationally challenging in the realm of many-body systems [10–12]. The underlying issue is the complexity of the minimization procedures required, which makes numerical evaluation intractable for systems larger than a few qubits. Recently, a significant advancement in overcoming this challenge has been marked by the development of more practical and computable measures. These include Bell magic [13], stabilizer nullity [14], and stabilizer Rényi entropies (SREs) [15]. Remarkable progress has also been achieved in the experimental measurement of these quantities, marking a notable step forward in the practical assessment of nonstabilizerness [16–21]. Among all these measures, SREs stand out for their favorable properties and computational tractability [15,22,23], making them the central focus of this work.

Despite these developments, much like the initial stages of understanding entanglement in many-body systems, the relationship between magic and physical phenomena (phase transition, criticality, etc.), as well as the interplay between magic and entanglement at the multiparticle level, remains largely unclear. A promising approach to address these questions lies in the use of tensor networks (TNs) [24–27]. They have currently offered the sole viable theoretical framework for computing magic on a large scale, employing both exact [28–30] and stochastic methods [22,31–34]. TN methods are, however, limited to systems with weak entanglement and in low dimensionality. In Ref. [35], the nonstabilizerness expressivity of some variational ansätze is examined for small system sizes.

In the present work, we go beyond the TN realm and extend the magic analysis to neural quantum states (NQS) [36]. Our contributions are threefold. First, we present methodologies to measure an SRE in quantum states encoded as NQS. Second, we apply these techniques to random NQS instances, showing that neural wave functions are able to capture a finite degree of nonstabilizerness besides extensive entanglement. Finally, we construct the magic phase diagram of the ground state of the one-dimensional (1D) and two-dimensional (2D) J_1-J_2 Heisenberg model, a paradigmatic quantum many-spin system

*Contact author: alessandro.sinibaldi@epfl.ch
†Contact author: amello@sissa.it

Published by the American Physical Society under the terms of the Creative Commons Attribution 4.0 International license. Further distribution of this work must maintain attribution to the author(s) and the published article's title, journal citation, and DOI.

that poses significant challenges for existing numerical methods. By leveraging the representative power of NQS ansätze, our approach effectively overcomes the limitations of state-of-the-art approaches for magic computation, enabling the investigation of nonstabilizerness in highly entangled many-body states in arbitrary spatial dimension. This opens new avenues for exploring the role of quantum resources in a plethora of physical scenarios.

II. NONSTABILIZERNESS RESOURCE THEORY

Here we consider a quantum system composed of N qubits (spins-$\frac{1}{2}$); extension to higher local dimension (qudits or larger spins) is straightforward. We define the set of Pauli matrices as $\{\hat{\sigma}^\mu\}_{\mu=0}^3$, where $\hat{\sigma}^0 = \hat{I}$ is the identity matrix. The local computational basis $\{|0\rangle, |1\rangle\}$ is given by the eigenstates of the Pauli matrix $\hat{\sigma}^3$, such that $\hat{\sigma}^3|\sigma\rangle = (-1)^\sigma|\sigma\rangle$ for $\sigma = 0, 1$. A general Pauli string $\hat{P}$ is identified by a set of indices $\boldsymbol{\mu} = \{\mu_1, \ldots, \mu_N\}$, with $\mu_j \in \{0, 1, 2, 3\}$ for $j = 1, \ldots, N$, such that $\hat{P}(\boldsymbol{\mu}) = \bigotimes_{j=1}^N \hat{\sigma}_j^{\mu_j} \in \mathcal{P}_N$. Here $\mathcal{P}_N$ encompasses all the possible Pauli strings with no overall phase. The N-qubit Pauli group is therefore defined as $\tilde{\mathcal{P}}_N = \{\pm 1, \pm i\} \times \mathcal{P}_N$.

Let us now introduce another important group that allows us to identify the magic resource in quantum systems. Among all possible unitary transformations that can be applied to a system of N qubits, there exists a special subset known as Clifford unitaries. These unitaries have the distinctive property of mapping Pauli strings to other Pauli strings, and they form a group. The Clifford group is thus defined as the normalizer of the Pauli group. It can be formally expressed as $\mathcal{C}_N = \{\hat{U} | \hat{U}\hat{P}\hat{U}^\dagger \in \tilde{\mathcal{P}}_N, \forall \hat{P} \in \tilde{\mathcal{P}}_N\}$ and can be generated using the Hadamard, phase, and cnot gate.

With all the essential elements at hand, we can define the *stabilizer states*: these are states that can be built solely through Clifford operations applied to the state $|0\rangle^{\otimes N}$. These particular states, despite their intricate architecture and the substantial entanglement introduced by cnot gates, do not provide any quantum advantage. The Gottesman-Knill theorem [4–6] reveals all the limitations of stabilizer states, demonstrating that Clifford circuits can be efficiently simulated on classical computers. This revelation underscores the inherent constraints of stabilizer states in the realm of quantum computation.

In this framework, it is essential to quantify the non-Clifford resources required to prepare a specific quantum state. The degree of nonstabilizerness, often referred to as magic, needs to be evaluated using appropriate measures. For a pure possibly non-normalized state $|\Psi\rangle$, the SREs [15] are a possible choice. These are defined as

$$M_\alpha = \frac{1}{1-\alpha} \log \left[\frac{1}{2^N} \sum_{\hat{P} \in \mathcal{P}_N} \left(\frac{\langle \Psi | \hat{P} | \Psi \rangle}{\langle \Psi | \Psi \rangle} \right)^{2\alpha} \right], \tag{1}$$

where α is the Rényi index. If we now introduce the probability distribution over $\mathcal{P}_N$:

$$\Xi_{\hat{P}} = \frac{1}{2^N} \left(\frac{\langle \Psi | \hat{P} | \Psi \rangle}{\langle \Psi | \Psi \rangle} \right)^2, \tag{2}$$

the SREs can be written as averages over this probability distribution:

$$M_\alpha = \frac{1}{1-\alpha} \log \mathbb{E}_{\hat{P} \sim \Xi_{\hat{P}}} \left[\Xi_{\hat{P}}^{\alpha-1} \right] - N \log 2, \quad \text{for } \alpha \neq 1, \tag{3a}$$

$$M_1 = -\mathbb{E}_{\hat{P} \sim \Xi_{\hat{P}}} [\log \Xi_{\hat{P}}] - N \log 2. \tag{3b}$$

Recent research has confirmed that for qubits and pure states, the SREs with $\alpha \geqslant 2$ exhibit monotonic behavior [23], meaning that they serve as valid measures of nonstabilizerness in a resource theory perspective. On the contrary, it has been observed that the monotonicity does not hold for $0 \leqslant \alpha < 2$, where violations are evident [22]. Therefore, in the following we consider $\alpha = 2$.

Multiple ways to efficiently estimate the SREs have been proposed, but each of these has a restricted validity. When the many-body quantum state $|\Psi\rangle$ can be effectively encoded as a matrix product state (MPS), there exist algorithms to calculate M_α directly from Eq. (1) [22,28,29]. These schemes inherit all the limitations of TN approaches, namely, they are efficiently applicable to low-entanglement systems and one-dimensional settings only. To overcome these limits, an approach based on quantum Monte Carlo (QMC) simulation has been proposed [37]. While this QMC method can handle systems in dimensions larger than one, its applicability is still constrained to wave functions that do not exhibit a sign problem [38]. Recently, an effective method for assessing nonstabilizerness in fermionic Gaussian states has also been introduced [39]. The most general approach to compute SREs remains, however, estimating them from Eq. (3), by performing a sampling in the space of Pauli strings $\mathcal{P}_N$ according to the probability distribution $\Xi_{\hat{P}}$ in Eq. (2). In the special case of an MPS ansatz, perfect sampling from exactly computable conditional probabilities can be performed [31,34]. For a generic quantum state with query and sampling access [40], one has to resort to Markov chain Monte Carlo in $\mathcal{P}_N$, as proposed in Ref. [32].

In this work, we present two methods based on Monte Carlo sampling of the wave function to estimate nonstabilizerness in arbitrary many-qubit systems. We call these two approaches *replicated estimator* and *Bell basis estimator*. In all the following, we denote as $\mathcal{H}$ the N-qubit Hilbert space and as $|\Psi\rangle$ the state for which we measure the nonstabilizerness.

III. REPLICATED ESTIMATOR

Consider the four times replicated Hilbert space $\bigotimes_{i=1}^4 \mathcal{H}$ with configurations $|\boldsymbol{\eta}\rangle = |\sigma^{(1)}, \sigma^{(2)}, \sigma^{(3)}, \sigma^{(4)}\rangle \equiv |\sigma^{(1)}\rangle \otimes |\sigma^{(2)}\rangle \otimes |\sigma^{(3)}\rangle \otimes |\sigma^{(4)}\rangle$, where $|\sigma^{(j)}\rangle \in \mathcal{H}$ for $j = 1, \ldots, 4$. Only for this estimator, we adopt the local spin basis $\{-1, 1\}$ instead of $\{0, 1\}$. Moreover, consider the quantum state

$$|\Phi\rangle = |\Psi^*, \Psi^*, \Psi^*, \Psi\rangle, \tag{4}$$

and the unitary operator defined by

$$\hat{U}|\boldsymbol{\eta}\rangle = |\sigma^{(2)} \odot \sigma^{(3)} \odot \sigma^{(4)}, \sigma^{(1)} \odot \sigma^{(3)} \odot \sigma^{(4)}, \sigma^{(1)} \odot \sigma^{(2)} \odot \sigma^{(4)}, \sigma^{(1)} \odot \sigma^{(2)} \odot \sigma^{(3)}\rangle, \tag{5}$$

where $\odot$ denotes the Hadamard product between the qubit strings. Using the results of Ref. [41], one can show that

$$\exp(-M_2) = \frac{\langle\Phi|\hat{U}|\Phi\rangle}{\langle\Phi|\Phi\rangle} = \mathbb{E}_{\boldsymbol{\eta}\sim|\Phi(\boldsymbol{\eta})|^2}\left[\frac{\langle\boldsymbol{\eta}|\hat{U}|\Phi\rangle}{\langle\boldsymbol{\eta}|\Phi\rangle}\right]. \quad (6)$$

Therefore, M_2 can be computed from an expectation value over $|\Phi\rangle$, which can be efficiently estimated by sampling from the distribution $|\langle\boldsymbol{\eta}|\Phi\rangle|^2/\langle\Phi|\Phi\rangle$. The details are reported in the Supplemental Material [42].

IV. BELL BASIS ESTIMATOR

The second method for computing nonstabilizerness is based on the equivalence between the expectation value of a Pauli string and the amplitude over a Bell state of two copies of the original system [9,13,43–45]. This estimator can be used only when $|\Psi\rangle$ is the ground state of a Hamiltonian $\hat{H}$. As shown in the Supplemental Material [42], we can write

$$\exp(-M_2) = \mathbb{E}_{\boldsymbol{\nu}\sim|\Gamma(\boldsymbol{\nu})|^2}\left[\frac{|\Gamma(\boldsymbol{\nu})|^2}{\Gamma(\boldsymbol{\nu}_0)^2}\right], \quad (7)$$

where $|\boldsymbol{\nu}\rangle$, $|\boldsymbol{\nu}_0\rangle \in \mathcal{H}\otimes\mathcal{H}$ with $|\boldsymbol{\nu}_0\rangle = |0,0,\ldots,0\rangle$ and $|\Gamma\rangle$ is the ground state of the transformed Hamiltonian $\hat{\mathbb{H}} = \hat{C}^\dagger(\hat{H}\otimes\hat{I} + \hat{I}\otimes\hat{H}^*)\hat{C}$, with $\hat{I}$ the identity and $\hat{C}$ a suitable Clifford transformation entangling the two copies of the system. In the same way as for Eq. (6), the average in Eq. (7) can be estimated via Monte Carlo sampling from $|\langle\boldsymbol{\nu}|\Gamma\rangle|^2/\langle\Gamma|\Gamma\rangle$.

In our framework, the states $|\Phi\rangle$ and $|\Gamma\rangle$ are encoded as suitable NQS. In general, the replicated estimator suffers from larger statistical fluctuations than the Bell basis estimator. This occurs because $\hat{U}$ in Eq. (5) is a nonlocal transformation, so $\langle\boldsymbol{\eta}|\hat{U}|\Phi\rangle$ and $\langle\boldsymbol{\eta}|\Phi\rangle$ can differ significantly, resulting in a stochastic estimate that is affected by statistical outliers. This is the same issue occurring in the Monte Carlo computation of the Rényi-2 entanglement entropy [46]. This problem, which is more severe for large system sizes, can be mitigated by increasing the number of effective samples with U statistics, as done in Ref. [47], or by employing a scheme inspired by annealed importance sampling [48], detailed in the Supplemental Material [42]. The Bell basis estimator is free from such a problem, since for it the distribution used in the sampling is proportional to the estimator itself. The sample complexities of the two estimators can be analyzed from the scaling of the statistical errors on M_2 with the system size N. As detailed in the Supplemental Material [42], the statistical errors are

$$\Delta M_2^{\text{repl.}} = \sqrt{\frac{e^{2M_2}-1}{N_s}}, \quad (8)$$

$$\Delta M_2^{\text{Bell}} = \sqrt{\frac{e^{2(M_2-M_3)}-1}{N_s}}, \quad (9)$$

where N_s is the number of samples used in the empirical averages. We note that, since the SREs satisfy the inequalities $M_\alpha \geqslant M_\beta$ for $\alpha < \beta$, the exponent in Eq. (9) is positive. Equations (8) and (9) entail that for both the estimators, if the SREs grow at most logarithmically with N, the number of samples N_s required to keep the errors fixed scales polynomial with N, meaning that the estimators are efficient. Logarithmic growth of SREs can arise in certain frustrated many-body systems [49]. Conversely, when the SREs scale linearly with N—as is typical for generic quantum many-body states—the numerators in Eqs. (8) and (9) grow exponentially with N, and so does the required number of samples N_s. Nevertheless, the sample complexity still grows substantially slower than the cost of an exact computation, which scales as 2^{2N}. In practice, these estimators remain valuable as they enable the exploration of system sizes that are otherwise intractable with exact methods. This is the same complexity as that of the Pauli-Markov chain method for the SREs [32] and the Monte Carlo estimation of the Rényi-2 entanglement entropy [46] for volume-law quantum states.

We remark that, while the replicated estimator is in general nonpositive, the Bell basis estimator is instead positive definite by construction and thus more robust for wave functions with sign structure. The Bell basis estimator, however, is limited to ground states and requires knowing the typically highly entangled state $|\Gamma\rangle$, which becomes challenging for complicated models. Even when the physical Hamiltonian $\hat{H}$ contains only local interactions, the Clifford transformation $\hat{C}$ introduces nonlocal couplings between the qubits of the system and those of the replica. Additionally, the interactions typically become more complex, with originally simple two-body terms in $\hat{H}$ transforming into higher-order interactions in $\hat{\mathbb{H}}$, often involving four-body couplings. This severely complicates learning the ground state of $\hat{\mathbb{H}}$ through variational Monte Carlo (VMC). Since these limitations are constraining for the applications we chose, we adopt the replicated estimator in all our calculations shown in the main text. The sketch in Fig. 1 pictorially illustrates the two approaches. In the Supplemental Material [42], we benchmark the two Monte Carlo estimators against a reference simulation performed with MPS.

V. ENSEMBLE OF RANDOM NQS

As a first application of the methods, we investigate the representative power of NQS in terms of nonstabilizerness. To do so, we analyze the magic content of an ensemble of NQS with random parameters. We consider the ensemble studied in Ref. [50] for entanglement properties, namely, a set of restricted Boltzmann machines (RBMs) [36] for N spins-$\frac{1}{2}$:

$$\Psi_\theta(\sigma) = e^{\sum_{i=1}^N a_i\sigma_i}\prod_{i=1}^M \cosh\left(\sum_{j=1}^N W_{ij}\sigma_j + b_i\right), \quad (10)$$

where the parameters $\theta = (a, b, W)$ are chosen such that the visible and hidden biases a and b are set to zero, while the complex weights W_{ij} are drawn uniformly from $[-3/N, 3/N]$ in the real part and from $[-\pi, \pi]$ in the imaginary part. The density of hidden neurons $\alpha = M/N$ is fixed to 1, since for this choice the average von Neumann entanglement entropy of the ensemble obeys a volume law, as shown in Ref. [50]. We compute the M_2 averaged over several independent realizations of these random RBMs for different numbers of spins N.

Figure 2 shows that for an enough large system size, the averaged M_2 of the ensemble increases linearly with N, as confirmed by the linear fit. Consequently, as displayed in the inset, the SRE density $m_2 = M_2/N$ converges to a finite value

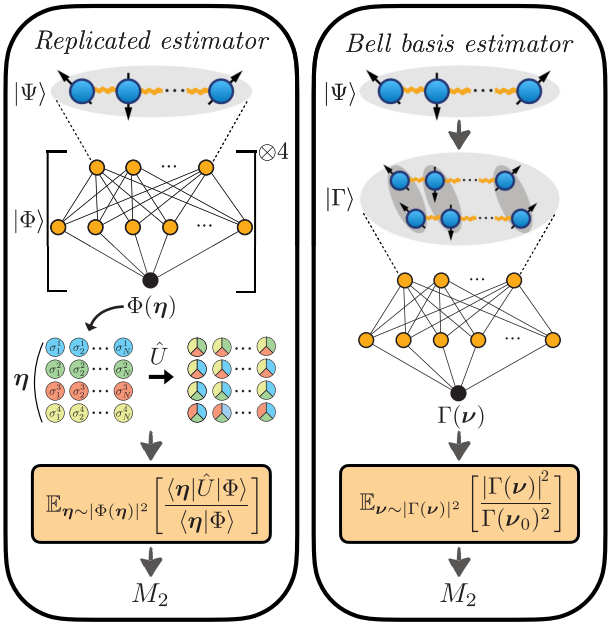


FIG. 1. Sketch of the two approaches for estimating the SRE M_2 of a many-qubit quantum state $|\Psi\rangle$ through Monte Carlo sampling. The replicated estimator consists of considering four unentangled copies of $|\Psi\rangle$ and sampling the expectation value of an operator $\hat{U}$ that creates interaction between the replicas. The Bell basis estimator involves two entangled copies of $|\Psi\rangle$ and computes the nonstabilizerness by averaging amplitude ratios. Each copy $|\Psi\rangle$ in the quadrupled state $|\Phi\rangle$ and the entire doubled entangled state $|\Gamma\rangle$ are encoded as NQS. The stochastic estimates of M_2 are performed by Monte Carlo sampling from the Born distributions of $|\Phi\rangle$ and $|\Gamma\rangle$.

in the thermodynamic limit, which corresponds to the slope of the fit since $m_2 = \gamma + \delta/N$. The asymptotic value is estimated as $m_2^* = \gamma = 0.241 \pm 0.005$ and quantifies the magic content in this ensemble of random NQS. This calculation shows that NQS parametrizations are capable of capturing finite nonstabilizerness besides large entanglement, simultaneously accounting for two distinct types of quantum resources.

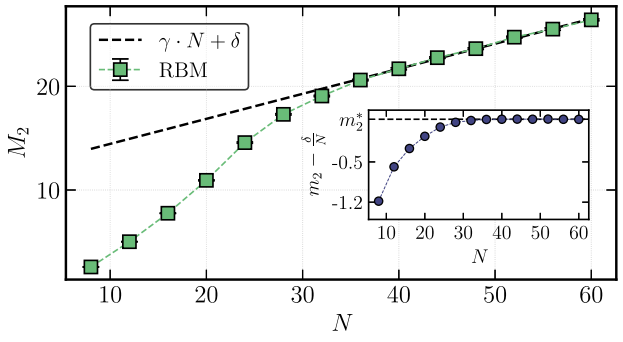


FIG. 2. Averaged SRE M_2 in the ensemble of random RBMs for various system sizes N. Each point is the mean over 10^3 independent realizations of the ensemble. The values of M_2 are estimated using $N_s = 2^{22} \approx 4 \times 10^6$ samples. The dashed line corresponds to a linear fit on the last seven data points. The inset displays the SRE density $m_2 = M_2/N$ without the offset coming from the intercept of the fit. The dashed line in the inset indicates the asymptotic value m_2^* of the SRE density for $N \to \infty$, which coincides with the slope of the fit.

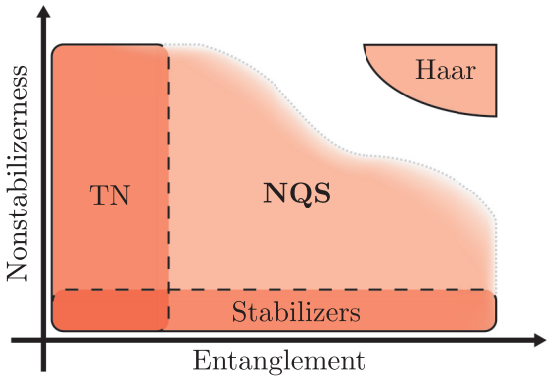


FIG. 3. Pictorial diagram illustrating the expressive power of some amplitude ratio quantum states [51] in terms of entanglement and nonstabilizerness. Here, TN indicates all the planar tensor network ansätze, including MPS as well as projected entangled pair states [62].

The scheme in Fig. 3 illustrates the representative power of NQS in terms of entanglement and magic content compared to other states of the amplitude ratio (AR) family [51]. This family comprises all states, generally non-normalized, from which one can sample and compute exponentially accurate amplitude ratios with polynomial complexity. TNs encompass states with low entanglement but arbitrarily high nonstabilizerness [52], while stabilizer states have no magic but are possibly highly entangled. NQS are known to represent any efficiently contracted TN wave function [53,54] and any stabilizer state [55–59]. Additionally, NQS can encode states with volume-law entanglement [50,60] and finite nonstabilizerness, as proved previously, as well as states with moderate entanglement but high magic content, as shown in the next section. Therefore, NQS allow us to represent AR states very close to random Haar states, which have nearly maximal values of both entanglement [61] and nonstabilizerness [52]. We note that the upper boundaries of NQS in Fig. 3 are speculative, as suggested by the faded edge, since it is still unknown whether NQS can represent random Haar states.

VI. J_1-J_2 HEISENBERG MODEL

We now explore the nonstabilizerness in the ground state of a paradigmatic quantum many-body spin system, the J_1-J_2 Heisenberg model with Hamiltonian

$$\hat{H} = J_1 \sum_{\langle i,j\rangle} \hat{\mathbf{S}}_i \cdot \hat{\mathbf{S}}_j + J_2 \sum_{\langle\langle i,j\rangle\rangle} \hat{\mathbf{S}}_i \cdot \hat{\mathbf{S}}_j, \tag{11}$$

where $\hat{\mathbf{S}}_i = (\hat{S}_i^x, \hat{S}_i^y, \hat{S}_i^z)$ is the spin-$\frac{1}{2}$ operator at site i, and $J_1, J_2 > 0$ are the antiferromagnetic couplings between nearest- and next-nearest-neighbor spins, respectively. We consider both a 1D spin chain and a 2D square lattice with periodic boundary conditions. The physical properties of the ground state of Eq. (11) have been extensively investigated over the years, with particular focus on the regime of high frustration, which has been revealed to be challenging for numerical methods [63–86]. It is therefore of particular interest to analyze the ground state in terms of nonstabilizer resources. Owing to the large entanglement of some phases

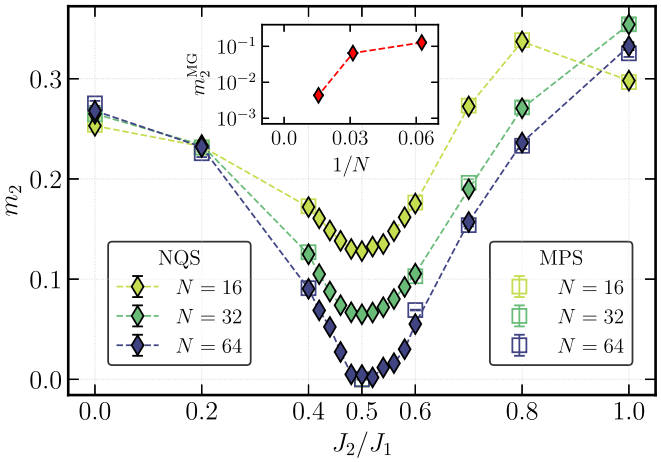


FIG. 4. SRE density m_2 in the ground state of the 1D J_1-J_2 Heisenberg model for different values of J_2/J_1. Results are shown for chains with $N = 16, 32, 64$ spins. The values of the SRE density are estimated using $N_s \approx 10^9$ samples. The inset shows the size scaling of m_2 at the Majumdar-Ghosh point $J_2 = J_1/2$, denoted as m_2^{MG}. The ground state is approximated using a complex RBM with $\alpha = 4$ for $N = 16$ and the ViT for $N = 32, 64$. The results from perfect sampling with MPS [31] using bond dimension $\chi = 400$ and $N_s = 10^4$ samples are reported as a benchmark.

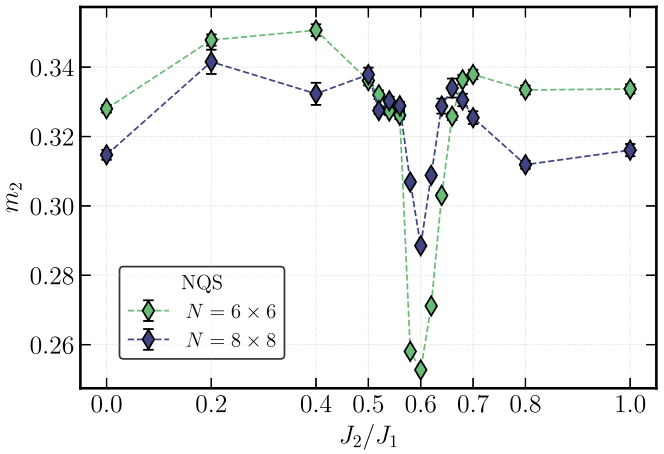


FIG. 5. SRE density m_2 in the ground state of the 2D J_1-J_2 Heisenberg model for different values of J_2/J_1. Results are shown for the 6×6 and the 8×8 lattices. The values of the SRE density are estimated using $N_s \approx 4 \times 10^6$ samples. The ground state is approximated by employing the ViT architecture.

and the possible high-dimensionality, standard TN approaches to compute nonstabilizerness [22,28–34] are impractical. On the other side, QMC-based schemes [37] are not applicable due to the nontrivial sign structure of the ground-state wave function for arbitrary couplings.

We approximate the ground state of Eq. (11) for different values of J_2/J_1 using variational Monte Carlo with a powerful NQS parametrization of the wave function. Specifically, we employ the deep vision transformer (ViT) architecture introduced in Refs. [83,87] together with the modern formulation of the stochastic reconfiguration [88,89] method in the limit of numerous variational parameters [84,85]. Some details on the ansatz and the optimization protocol are reported in the Supplemental Material [42]. Once we obtain the ground states, we compute M_2 for each of them.

Since we cannot access the exact wave function for the considered system sizes, it is imperative to quantify the variational error committed on the SRE due to the NQS approximation of the ground state. The calculation for m_2 is shown in the Supplemental Material [42], and it follows that its variational error is estimated at leading order as $\sqrt{\mathrm{Var}(\hat{H})}/N$, where $\mathrm{Var}(\hat{H})$ is the energy variance on the optimized NQS. From the Monte Carlo calculation of the variance, we can therefore estimate the systematic error on m_2 due to the variational approximation.

Figure 4 reveals that in the 1D system m_2 attains a minimum in correspondence of $J_2 = J_1/2$, namely, when the 1D J_1-J_2 Heisenberg model corresponds to the exactly solvable Majumdar-Ghosh (MG) model [90]. In particular, the minimum of the SRE density approaches zero as the system size increases, as shown in the inset. This is in perfect agreement with what is expected from the MG ground state, since it is known that this consists of a valence bond state composed of singlets of maximally entangled spins, which is a stabilizer. With periodic boundary conditions, the actual ground state is, in general, a superposition of two degenerate ground states that differ by translating the singlets by one lattice spacing. Therefore, the nonstabilizerness can be small yet nonvanishing at finite size. However, as we approach the thermodynamic limit, the degeneracy disappears and the ground state becomes a single stabilizer. The results from MPS calculations [31] closely match those from NQS across the full phase diagram, confirming the accuracy of our findings for the 1D system.

For the 2D model, as displayed in Fig. 5, m_2 shows a clear dip in the regime of maximum frustration reaching a finite minimum around $J_2/J_1 \approx 0.6$. This behavior is reminiscent of the 1D case in Fig. 4, but differs since the minimal m_2 remains nonvanishing as we increase the system size. What is observed in the 2D model around $J_2/J_1 \approx 0.6$ is compatible with a valence bond solid (VBS) phase up to some finite-size correction, which implies a reduction of the nonstabilizerness without complete cancellation. The presence of the VBS between the Néel (small J_2/J_1) and the stripe-type (large J_2/J_1) antiferromagnetic orders in the 2D J_1-J_2 model has been proposed in several previous works [66,67,69,70,75]. For the 2D system, TNs cannot serve as a reliable benchmark, as NQS have demonstrated superior accuracy in capturing the ground state [85]. Even when accurate TN approximations are attainable [66,91], the large bond dimension χ required renders the computation of the SRE practically infeasible. Indeed, the scaling with χ of TN-based algorithms for estimating M_2, such as the MPS perfect sampling [31] with $O(N_s N \chi^3)$, the replica approach [28] with $O(N\chi^{12})$, and the Pauli-Markov chain method [32] with $O(\log N \chi^4)$, limits computations to small bond dimensions, for which the ground-state approximation becomes inadequate.

VII. OUTLOOK AND CONCLUSIONS

In this work, we introduce a framework for quantifying nonstabilizerness in terms of stabilizer Rényi entropies with neural quantum states. We present two Monte Carlo

algorithms to measure nonstabilizerness in quantum many-body states encoded in arbitrary variational ansätze. Combining these schemes with NQS enables overcoming the limitations of TN methods imposed by extensive correlations and high dimensionality. First, we characterize the magic content of random NQS wave functions, proving that neural network parametrizations are able to capture multiple quantum resources simultaneously, namely, both finite nonstabilizerness and large entanglement. Second, we compute the SRE in the ground state of the J_1-J_2 Heisenberg model on the spin chain and on the square lattice. This frustrated quantum spin system cannot be efficiently addressed with state-of-the-art approaches for magic computation. Our simulations show that in 1D the nonstabilizerness decreases to zero at $J_2 = J_1/2$ in the thermodynamic limit, which is in agreement with the stabilizer nature of the Majumdar-Ghosh ground state. In 2D, instead, the SRE displays a clear dip in the regime of maximum frustration with a nonvanishing minimum around $J_2/J_1 \approx 0.6$. This diminution in the nonstabilizerness aligns with the presence of a valence bond solid phase in the intermediate region between the two antiferromagnetic ordered regimes.

A potential development of this work is extending the magic analysis to interacting fermionic systems. Additionally, an important direction is the investigation of the nonstabilizerness dynamics in the time evolution of strongly correlated quantum systems simulated with NQS methods [36,92–96]. Finally, it is relevant to thoroughly assess the capability of NQS to represent states with maximal quantum complexity, namely, those that simultaneously saturate both entanglement and nonstabilizerness, akin to random Haar states.

ACKNOWLEDGMENTS

We warmly thank V. Savona, M. Dalmonte, P. Tarabunga, and G. Lami for inspirational and insightful discussions. We gratefully acknowledge Luciano Loris Viteritti and Riccardo Rende for providing the code of the ViT ansatz and assisting in its VMC optimization. A.S. was supported by SEFRI under Grant No. MB22.00051 (NEQS—Neural Quantum Simulation). The Flatiron Institute is a division of the Simons Foundation. M.C. thanks support by the PNRR MUR Project No. PE0000023-NQSTI and the PRIN 2022 (2022R35ZBF)—PE2—"ManyQLowD."

DATA AVAILABILITY

The code for the simulations is based on the software package NetKet [97,98] and is available at [99]. We acknowledge the use of Stim [100] for the stabilizer formalism operations, and of ITensor [101] for the MPS calculations.

[1] J. Eisert, M. Cramer, and M. B. Plenio, *Colloquium*: Area laws for the entanglement entropy, Rev. Mod. Phys. **82**, 277 (2010).
[2] J. I. Cirac and P. Zoller, Goals and opportunities in quantum simulation, Nat. Phys. **8**, 264 (2012).
[3] A. A. Houck, H. E. Türeci, and J. Koch, On-chip quantum simulation with superconducting circuits, Nat. Phys. **8**, 292 (2012).
[4] D. Gottesman, Stabilizer codes and quantum error correction, arXiv:quant-ph/9705052.
[5] D. Gottesman, The Heisenberg representation of quantum computers, arXiv:quant-ph/9807006.
[6] S. Aaronson and D. Gottesman, Improved simulation of stabilizer circuits, Phys. Rev. A **70**, 052328 (2004).
[7] D. Gross, Non-negative Wigner functions in prime dimensions, Appl. Phys. B **86**, 367 (2007).
[8] V. Veitch, C. Ferrie, D. Gross, and J. Emerson, Negative quasi-probability as a resource for quantum computation, New J. Phys. **14**, 113011 (2012).
[9] D. Gross, S. Nezami, and M. Walter, Schur–Weyl duality for the Clifford group with applications: Property testing, a robust Hudson theorem, and de Finetti representations, Commun. Math. Phys. **385**, 1325 (2021).
[10] M. Howard and E. Campbell, Application of a resource theory for magic states to fault-tolerant quantum computing, Phys. Rev. Lett. **118**, 090501 (2017).
[11] S. Bravyi, D. Browne, P. Calpin, E. Campbell, D. Gosset, and M. Howard, Simulation of quantum circuits by low-rank stabilizer decompositions, Quantum **3**, 181 (2019).
[12] M. Heinrich and D. Gross, Robustness of magic and symmetries of the stabiliser polytope, Quantum **3**, 132 (2019).
[13] T. Haug and M. Kim, Scalable measures of magic resource for quantum computers, PRX Quantum **4**, 010301 (2023).
[14] M. Beverland, E. Campbell, M. Howard, and V. Kliuchnikov, Lower bounds on the non-Clifford resources for quantum computations, Quantum Sci. Technol. **5**, 035009 (2020).
[15] L. Leone, S. F. E. Oliviero, and A. Hamma, Stabilizer Rényi entropy, Phys. Rev. Lett. **128**, 050402 (2022).
[16] S. F. E. Oliviero, L. Leone, A. Hamma, and S. Lloyd, Measuring magic on a quantum processor, npj Quantum Inf. **8**, 148 (2022).
[17] P. Niroula, C. D. White, Q. Wang, S. Johri, D. Zhu, C. Monroe, C. Noel, and M. J. Gullans, Phase transition in magic with random quantum circuits, Nat. Phys. **20**, 1786 (2024).
[18] D. Bluvstein, S. J. Evered, A. A. Geim, S. H. Li, H. Zhou, T. Manovitz, S. Ebadi, M. Cain, M. Kalinowski, D. Hangleiter *et al.*, Logical quantum processor based on reconfigurable atom arrays, Nature (London) **626**, 58 (2024).
[19] S. Bera and M. Schirò, Non-stabilizerness of Sachdev-Ye-Kitaev model, arXiv:2502.01582 [quant-ph].
[20] R. Smith, Z. Papić, and A. Hallam, Non-stabilizerness in kinetically-constrained Rydberg atom arrays, Phys. Rev. B **111**, 245148 (2025).
[21] N. Dowling, K. Modi, and G. A. L. White, Bridging entanglement and magic resources within operator space, Phys. Rev. Lett. **135**, 160201 (2025).
[22] T. Haug and L. Piroli, Stabilizer entropies and nonstabilizerness monotones, Quantum **7**, 1092 (2023).
[23] L. Leone and L. Bittel, Stabilizer entropies are monotones for magic-state resource theory, Phys. Rev. A **110**, L040403 (2024).

[24] S. R. White, Density matrix formulation for quantum renormalization groups, Phys. Rev. Lett. **69**, 2863 (1992).

[25] R. Orús, A practical introduction to tensor networks: Matrix product states and projected entangled pair states, Ann. Phys. **349**, 117 (2014).

[26] A. F. Mello, A. Santini, and M. Collura, Hybrid stabilizer matrix product operator, Phys. Rev. Lett. **133**, 150604 (2024).

[27] A. F. Mello, A. Santini, G. Lami, J. D. Nardis, and M. Collura, Clifford dressed time-dependent variational principle, Phys. Rev. Lett. **134**, 150403 (2025).

[28] T. Haug and L. Piroli, Quantifying nonstabilizerness of matrix product states, Phys. Rev. B **107**, 035148 (2023).

[29] P. S. Tarabunga, E. Tirrito, M. C. Bañuls, and M. Dalmonte, Nonstabilizerness via matrix product states in the Pauli basis, Phys. Rev. Lett. **133**, 010601 (2024).

[30] A. Paviglianiti, G. Lami, M. Collura, and A. Silva, Estimating non-stabilizerness dynamics without simulating it, PRX Quantum **6**, 030320 (2025).

[31] G. Lami and M. Collura, Nonstabilizerness via perfect Pauli sampling of matrix product states, Phys. Rev. Lett. **131**, 180401 (2023).

[32] P. S. Tarabunga, E. Tirrito, T. Chanda, and M. Dalmonte, Many-body magic via Pauli-Markov chains—From criticality to gauge theories, PRX Quantum **4**, 040317 (2023).

[33] P. S. Tarabunga, Critical behaviours of non-stabilizerness in quantum spin chains, Quantum **8**, 1413 (2024).

[34] G. Lami and M. Collura, Unveiling the stabilizer group of a matrix product state, Phys. Rev. Lett. **133**, 010602 (2024).

[35] T. Spriggs, A. Ahmadi, B. Chen, and E. Greplova, Quantum resources of quantum and classical variational methods, Mach. Learn.: Sci. Technol. **6**, 015042 (2025).

[36] G. Carleo and M. Troyer, Solving the quantum many-body problem with artificial neural networks, Science **355**, 602 (2017).

[37] Z. Liu and B. K. Clark, Non-equilibrium quantum Monte Carlo algorithm for stabilizer Renyi entropy in spin systems, Phys. Rev. B **111**, 085144 (2025).

[38] M. Troyer and U.-J. Wiese, Computational complexity and fundamental limitations to fermionic quantum Monte Carlo simulations, Phys. Rev. Lett. **94**, 170201 (2005).

[39] M. Collura, J. D. Nardis, V. Alba, and G. Lami, The quantum magic of fermionic Gaussian states, arXiv:2412.05367 [quant-ph].

[40] M. V. den Nest, Simulating quantum computers with probabilistic methods, arXiv:0911.1624 [quant-ph].

[41] P. S. Tarabunga and C. Castelnovo, Magic in generalized Rokhsar-Kivelson wavefunctions, Quantum **8**, 1347 (2024).

[42] See Supplemental Material at http://link.aps.org/supplemental/10.1103/v5tw-yn1f for additional details on the two Monte Carlo estimators for the SRE M_2 and their benchmark against MPS, the annealed importance sampling scheme, the optimization of the deep ViT ansatz, and the variational error on the SRE density, which also includes Refs. [102–107].

[43] A. Montanaro, Learning stabilizer states by Bell sampling, arXiv:1707.04012 [quant-ph].

[44] C.-Y. Lai and H.-C. Cheng, Learning quantum circuits of some T gates, IEEE Trans. Inf. Theory **68**, 3951 (2022).

[45] T. Haug, S. Lee, and M. S. Kim, Efficient quantum algorithms for stabilizer entropies, Phys. Rev. Lett. **132**, 240602 (2024).

[46] M. B. Hastings, I. González, A. B. Kallin, and R. G. Melko, Measuring Renyi entanglement entropy in quantum Monte Carlo simulations, Phys. Rev. Lett. **104**, 157201 (2010).

[47] P. R. N. Falcão, P. S. Tarabunga, M. Frau, E. Tirrito, J. Zakrzewski, and M. Dalmonte, Non-stabilizerness in U(1) lattice gauge theory, Phys. Rev. B **111**, L081102 (2025).

[48] R. M. Neal, Annealed importance sampling, Stat. Comput. **11**, 125 (2001).

[49] J. Odavić, T. Haug, G. Torre, A. Hamma, F. Franchini, and S. M. Giampaolo, Complexity of frustration: A new source of non-local non-stabilizerness, SciPost Phys. **15**, 131 (2023).

[50] D.-L. Deng, X. Li, and S. Das Sarma, Quantum entanglement in neural network states, Phys. Rev. X **7**, 021021 (2017).

[51] V. Havlicek, Amplitude ratios and neural network quantum states, Quantum **7**, 938 (2023).

[52] G. Lami, T. Haug, and J. De Nardis, Quantum state designs with Clifford enhanced matrix product states, PRX Quantum **6**, 010345 (2025).

[53] O. Sharir, A. Shashua, and G. Carleo, Neural tensor contractions and the expressive power of deep neural quantum states, Phys. Rev. B **106**, 205136 (2022).

[54] D. Wu, R. Rossi, F. Vicentini, and G. Carleo, From tensor-network quantum states to tensorial recurrent neural networks, Phys. Rev. Res. **5**, L032001 (2023).

[55] Y.-H. Zhang, Z. Jia, Y.-C. Wu, and G.-C. Guo, An efficient algorithmic way to construct Boltzmann machine representations for arbitrary stabilizer code, arXiv:1809.08631 [quant-ph].

[56] Z.-A. Jia, Y.-H. Zhang, Y.-C. Wu, L. Kong, G.-C. Guo, and G.-P. Guo, Efficient machine-learning representations of a surface code with boundaries, defects, domain walls, and twists, Phys. Rev. A **99**, 012307 (2019).

[57] S. Lu, X. Gao, and L.-M. Duan, Efficient representation of topologically ordered states with restricted Boltzmann machines, Phys. Rev. B **99**, 155136 (2019).

[58] Y. Zheng, H. He, N. Regnault, and B. A. Bernevig, Restricted Boltzmann machines and matrix product states of one-dimensional translationally invariant stabilizer codes, Phys. Rev. B **99**, 155129 (2019).

[59] M. Y. Pei and S. R. Clark, Compact neural-network quantum state representations of Jastrow and stabilizer states, J. Phys. A: Math. Theor. **54**, 405304 (2021).

[60] Z. Denis, A. Sinibaldi, and G. Carleo, Comment on "Can neural quantum states learn volume-law ground states?" Phys. Rev. Lett. **134**, 079701 (2025).

[61] D. N. Page, Average entropy of a subsystem, Phys. Rev. Lett. **71**, 1291 (1993).

[62] F. Verstraete and J. I. Cirac, Renormalization algorithms for quantum-many body systems in two and higher dimensions, arXiv:cond-mat/0407066.

[63] S. Eggert, Numerical evidence for multiplicative logarithmic corrections from marginal operators, Phys. Rev. B **54**, R9612 (1996).

[64] S. R. White and I. Affleck, Dimerization and incommensurate spiral spin correlations in the zigzag spin chain: Analogies to the Kondo lattice, Phys. Rev. B **54**, 9862 (1996).

[65] W.-J. Hu, F. Becca, A. Parola, and S. Sorella, Direct evidence for a gapless Z_2 spin liquid by frustrating Néel antiferromagnetism, Phys. Rev. B **88**, 060402 (2013).

[66] S.-S. Gong, W. Zhu, D. N. Sheng, O. I. Motrunich, and M. P. A. Fisher, Plaquette ordered phase and quantum phase diagram in the spin-$\frac{1}{2}$ J_1-J_2 square Heisenberg model, Phys. Rev. Lett. **113**, 027201 (2014).

[67] S. Morita, R. Kaneko, and M. Imada, Quantum spin liquid in spin 1/2 J_1-J_2 Heisenberg model on square lattice: Many-variable variational Monte Carlo study combined with quantum-number projections, J. Phys. Soc. Jpn. **84**, 024720 (2015).

[68] X. Liang, W.-Y. Liu, P.-Z. Lin, G.-C. Guo, Y.-S. Zhang, and L. He, Solving frustrated quantum many-particle models with convolutional neural networks, Phys. Rev. B **98**, 104426 (2018).

[69] L. Wang and A. W. Sandvik, Critical level crossings and gapless spin liquid in the square-lattice spin-1/2 J_1-J_2 Heisenberg antiferromagnet, Phys. Rev. Lett. **121**, 107202 (2018).

[70] R. Haghshenas and D. N. Sheng, $U(1)$-symmetric infinite projected entangled-pair states study of the spin-1/2 square J_1-J_2 Heisenberg model, Phys. Rev. B **97**, 174408 (2018).

[71] F. Ferrari, F. Becca, and J. Carrasquilla, Neural Gutzwiller-projected variational wave functions, Phys. Rev. B **100**, 125131 (2019).

[72] K. Choo, T. Neupert, and G. Carleo, Two-dimensional frustrated J_1-J_2 model studied with neural network quantum states, Phys. Rev. B **100**, 125124 (2019).

[73] A. Szabó and C. Castelnovo, Neural network wave functions and the sign problem, Phys. Rev. Res. **2**, 033075 (2020).

[74] X. Liang, S.-J. Dong, and L. He, Hybrid convolutional neural network and projected entangled pair states wave functions for quantum many-particle states, Phys. Rev. B **103**, 035138 (2021).

[75] Y. Nomura and M. Imada, Dirac-type nodal spin liquid revealed by refined quantum many-body solver using neural-network wave function, correlation ratio, and level spectroscopy, Phys. Rev. X **11**, 031034 (2021).

[76] L. L. Viteritti, F. Ferrari, and F. Becca, Accuracy of restricted Boltzmann machines for the one-dimensional J_1-J_2 Heisenberg model, SciPost Phys. **12**, 166 (2022).

[77] H. Chen, D. Hendry, P. Weinberg, and A. E. Feiguin, Systematic improvement of neural network quantum states using a Lanczos recursion, in *Proceedings of the 36th International Conference on Neural Information Processing Systems*, *NIPS '22* (Curran Associates Inc., Red Hook, NY, 2024).

[78] M. Li, J. Chen, Q. Xiao, F. Wang, Q. Jiang, X. Zhao, R. Lin, H. An, X. Liang, and L. He, Bridging the gap between deep learning and frustrated quantum spin system for extreme-scale simulations on new generation of sunway supercomputer, IEEE Trans. Parallel Distrib. Syst. **33**, 2846 (2022).

[79] C. Roth, A. Szabó, and A. H. MacDonald, High-accuracy variational Monte Carlo for frustrated magnets with deep neural networks, Phys. Rev. B **108**, 054410 (2023).

[80] X. Liang, M. Li, Q. Xiao, J. Chen, C. Yang, H. An, and L. He, Deep learning representations for quantum many-body systems on heterogeneous hardware, Mach. Learn.: Sci. Technol. **4**, 015035 (2023).

[81] E. Ledinauskas and E. Anisimovas, Scalable imaginary time evolution with neural network quantum states, SciPost Phys. **15**, 229 (2023).

[82] M. Reh, M. Schmitt, and M. Gärttner, Optimizing design choices for neural quantum states, Phys. Rev. B **107**, 195115 (2023).

[83] L. L. Viteritti, R. Rende, and F. Becca, Transformer variational wave functions for frustrated quantum spin systems, Phys. Rev. Lett. **130**, 236401 (2023).

[84] A. Chen and M. Heyl, Empowering deep neural quantum states through efficient optimization, Nat. Phys. **20**, 1476 (2024).

[85] R. Rende, L. L. Viteritti, L. Bardone, F. Becca, and S. Goldt, A simple linear algebra identity to optimize large-scale neural network quantum states, Commun. Phys. **7**, 260 (2024).

[86] J.-Q. Wang, H.-Q. Wu, R.-Q. He, and Z.-Y. Lu, Variational optimization of the amplitude of neural-network quantum many-body ground states, Phys. Rev. B **109**, 245120 (2024).

[87] L. L. Viteritti, R. Rende, A. Parola, S. Goldt, and F. Becca, Transformer wave function for two dimensional frustrated magnets: Emergence of a spin-liquid phase in the Shastry-Sutherland model, Phys. Rev. B **111**, 134411 (2025).

[88] S. Sorella, Green function Monte Carlo with stochastic reconfiguration, Phys. Rev. Lett. **80**, 4558 (1998).

[89] S. Sorella, Wave function optimization in the variational Monte Carlo method, Phys. Rev. B **71**, 241103 (2005).

[90] C. K. Majumdar and D. K. Ghosh, On next-nearest-neighbor interaction in linear chain. I, J. Math. Phys. **10**, 1388 (1969).

[91] X. Qian and M. Qin, Absence of spin liquid phase in the J_1-J_2 Heisenberg model on the square lattice, Phys. Rev. B **109**, L161103 (2024).

[92] M. Schmitt and M. Heyl, Quantum many-body dynamics in two dimensions with artificial neural networks, Phys. Rev. Lett. **125**, 100503 (2020).

[93] A. Sinibaldi, C. Giuliani, G. Carleo, and F. Vicentini, Unbiasing time-dependent variational Monte Carlo by projected quantum evolution, Quantum **7**, 1131 (2023).

[94] L. Gravina, V. Savona, and F. Vicentini, Neural projected quantum dynamics: A systematic study, Quantum **9**, 1803 (2025).

[95] A. Sinibaldi, D. Hendry, F. Vicentini, and G. Carleo, Time-dependent neural Galerkin method for quantum dynamics, arXiv:2412.11778 [quant-ph].

[96] J. Nys, G. Pescia, A. Sinibaldi, and G. Carleo, *Ab-initio* variational wave functions for the time-dependent many-electron Schrödinger equation, Nat. Commun. **15**, 9404 (2024).

[97] G. Carleo *et al.*, NetKet: A machine learning toolkit for many-body quantum systems, SoftwareX **10** 100311 (2019).

[98] F. Vicentini *et al.*, NetKet 3: Machine learning toolbox for many-body quantum systems, SciPost Phys. Codebases 7 (2022).

[99] A. Sinibaldi, cqsl/nqsmagic: First release, Zenodo (2025), doi: 10.5281/zenodo.16941784.

[100] C. Gidney, Stim: A fast stabilizer circuit simulator, Quantum **5**, 497 (2021).

[101] M. Fishman, S. R. White, and E. M. Stoudenmire, The ITensor software library for tensor network calculations, SciPost Phys. Codebases 4 (2022).

[102] G. B. Mbeng, A. Russomanno, and G. E. Santoro, The quantum Ising chain for beginners, SciPost Phys. Lect. Notes 82 (2024).

[103] S. F. E. Oliviero, L. Leone, and A. Hamma, Magic-state resource theory for the ground state of the transverse-field Ising model, Phys. Rev. A **106**, 042426 (2022).

[104] Z. Liu, H. Mao, C.-Y. Wu, C. Feichtenhofer, T. Darrell, and S. Xie, A ConvNet for the 2020s, in *Proceedings of the IEEE/CVF Conference on Computer Vision and Pattern Recognition* (2022), pp. 11976–11986.

[105] Y. Bengio, A. Courville, and P. Vincent, Representation learning: A review and new perspectives, IEEE Trans. Pattern Anal. Mach. Intell. **35**, 1798 (2013).

[106] Z. Denis and G. Carleo, Accurate neural quantum states for interacting lattice bosons, Quantum **9**, 1772 (2025).

[107] W. Marshall, Antiferromagnetism, Proc. R. Soc. London A **232**, 48 (1955).